Observation of Anti-Stokes Fluorescence Cooling in Thulium-Doped Glass

C. W. Hoyt* and M. Sheik-Bahae
Optical Sciences and Engineering, Department of Physics and Astronomy, University of New Mexico, Albuquerque, New Mexico 87131

R. I. Epstein, B. C. Edwards, and J. E. Anderson
Los Alamos National Laboratory, Los Alamos, New Mexico 87545
(Received 28 June 2000)

We report the first observation of anti-Stokes fluorescence cooling in a thulium-doped solid with pump excitation at 1.82 μm $< \lambda <$ 1.97 μm. At a pump wavelength of 1.9 μm and incident average power of $\sim$3 W, a Tm^{3+}:ZBLANP (ZrF_4-BaF_2-LaF_3-AlF_3-NaF-PbF_2) sample cooled to $-1.2\,^\circ$C from room temperature for a single pass of the pump beam. This corresponds to an absorbed pump power of $\sim$40 mW and a peak temperature change per absorbed power of $\sim -30\,^\circ$C/W from room temperature.

PACS numbers: 32.80.Pj, 42.55.Rz, 44.40.+a, 78.55.Hx

Parallel to advances in laser cooling of atoms and ions in dilute gas phase, major experimental progress has recently been made in laser cooling of matter in solid and liquid phases [1,2]. Laser refrigeration of solids can potentially lead to the development of an all solid-state cryocooler that can be used for a variety of applications such as cooling sensors and electronics [3]. Since the first observation of optical refrigeration in a solid (ytterbium-doped glass) in 1995 by Epstein *et al.* [1], researchers have made major strides toward achieving laser induced solid-state cryocoolers [4]. Ytterbium-doped glass has been cooled by more than 50 K below room temperature and has been shown to cool at 100 K [3,5,6]. Progress has been made toward cooling semiconductor materials although no net cooling has yet been observed due to radiation trapping [7,8]. Here we report the first demonstration of laser induced cooling of a thulium-doped glass—the second solid after Yb^{3+}-doped glass to exhibit net bulk cooling. These measurements allow us to test material scalability such as the predicted increase in cooling efficiency with decreasing pump photon energy. Moreover, unlike in Yb^{3+}-doped systems, these results demonstrate anti-Stokes fluorescence cooling in the presence of excited-state absorption.

We studied a number of Tm^{3+}-doped glasses and crystals (CaF_2, BaF_2, YAlO, LuAG, ZBLANP) but only one, a ZBLANP (ZrF_4-BaF_2-LaF_3-AlF_3-NaF-PbF_2) sample, exhibited a net cooling effect. This sample consisted of high purity 1 wt% Tm^{3+}:ZBLANP cut from a fiber preform. The relevant energy manifolds for Tm^{3+} ions in this host are shown in Fig. 1 [9]. Each level corresponds to a Stark-split manifold of several inhomogeneously broadened levels. We use the transitions between the $^3H_6$ and $^3H_4$ manifolds for our cooling cycle.

The cooling cycle in anti-Stokes fluorescence cooling involves pump excitation, thermalization, and spontaneous decay. As shown in Fig. 1, laser pump photons excite the dopant ensemble from the top of the ground-state manifold to the bottom of the excited-state manifold. The excitations thermalize within the upper and lower manifolds. The atoms decay through spontaneous emission (fluorescence) with a mean energy of $h\nu_f$, where ν_f is the mean fluorescent frequency. For each absorbed pump photon of energy $h\nu$, an average energy $h\nu_f - h\nu$ is removed from the thermal vibrations in the glass and carried out of the system. The cooling efficiency can be defined as the ratio of the cooling power to absorbed power and by energy considerations is

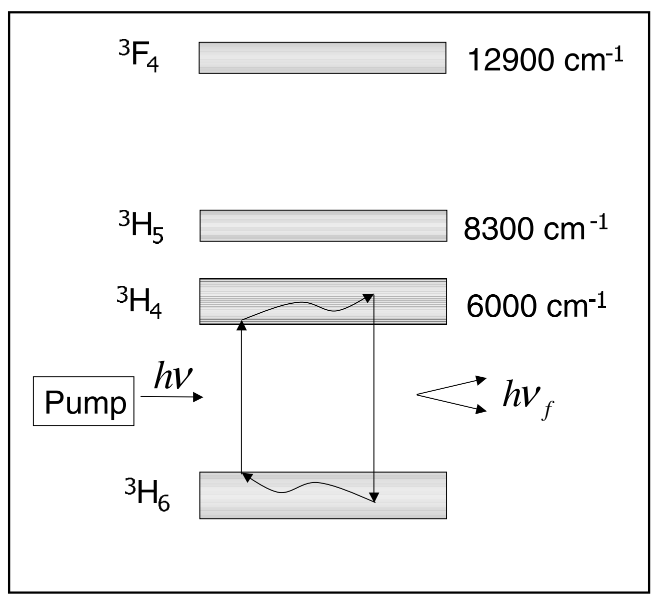

FIG. 1. Energy manifold diagram of Tm^{3+}:ZBLANP after Ref. [9]. The dopant ensemble is excited by the pump from the top of the ground-state manifold ($^3H_6$) to the bottom of the excited state manifold ($^3H_4$). The atoms thermalize in both manifolds by absorbing vibrational energy from the host, which, on the average, removes an energy $h\nu_f - h\nu$ for each absorbed photon.

 0031-9007/00/85(17)/3600(4)$15.00

$$\eta_{\mathrm{cooling}} = \frac{\nu_f - \nu}{\nu} = \frac{\lambda - \lambda_f}{\lambda_f}, \tag{1}$$

where λ and λ_f are the pump and mean fluorescent wavelengths, respectively. Figure 2 shows the emission spectrum and mean fluorescent wavelength (λ_f) of a Tm^{3+}:ZBLANP sample after Ref. [10]. Also shown in the figure is the absorptivity of our Tm^{3+}:ZBLANP sample as taken with a Fourier transform infrared spectrophotometer. Equation (1) describes the fundamental limit on the cooler performance. It suggests that, for a given material, longer pump wavelengths produce higher efficiencies. In practice, however, diminished pump absorption at long wavelengths due to the thermal distribution of the ground-state population limits the useful pump wavelength. Moreover, as discussed below, the ever present parasitic absorption due to unwanted impurities in the material further limits the effective range of long-wavelength excitations. The practical range of the energy difference $h\nu_f - h\nu$ is at most a few times thermal energy (kT) as a consequence of the ground-state Boltzman distribution. Therefore, with $h\nu_f - h\nu = \beta kT$, where β is determined by device design and geometries, Eq. (1) indicates that Tm^{3+}-doped materials with $h\nu_f \approx 0.7$ eV have the potential to cool nearly twice as efficiently as Yb^{3+}-doped materials with $h\nu_f \approx 1.25$ eV [1].

Although dopant ions with lower energy gaps can produce more efficient cooling, they will generally be subject to higher nonradiative decay rates that are strongly host dependent. For the relevant energy gaps, multiphonon assisted transition probabilities (rates) increase exponentially with decreasing energy gap. These rates vary greatly from host to host because of the large diversity in phonon energy spectra. Figure 3 is a logarithmic plot of nonradiative decay rate versus energy gap for a number of different hosts [11]. The $^3H_6 \rightarrow {}^3H_4$ energy gap in a fluorozirconate host such as ZBLANP ($\sim$5000 cm^{-1} for transitions most important for heating considerations) corresponds to $\sim 10^{-1}$ s^{-1} which is $\sim 10^{-4}$ times the radiative rate of $\sim$160 s^{-1} [11]. The resultant heating due to nonradiative processes in pure Tm^{3+}:ZBLANP should be insignificant.

The tunable pump source for our experiments was an optical parametric oscillator (OPO) based on periodically poled lithium niobate, synchronously pumped by a 20 W cw-mode-locked Nd:YAG laser (Coherent Antares). The OPO was operated singly resonant and had a maximum average output power of 6.2 W, signal tunability between 1.75–2.05 μm, and a signal output slope efficiency of 42% [12]. The pump beam was focused into the sample ($5 \times 5 \times 9$ mm^3) that rested on thin glass support slides in a vacuum chamber at approximately 10^{-5} Torr. An identical reference sample was also placed in the chamber on separate slides out of the beam path. We recorded the net temperature change of the sample relative to the reference sample using a pyroelectric thermal camera (ISI Group). The samples were observed through a CaF_2 window in the chamber for a single pass of the pump beam at a given wavelength after the sample reached thermal equilibrium with its surroundings inside the vacuum chamber. We calibrated the thermal camera by controlling the temperature of a similar glass sample: for a particular aperture of the camera the digitized image yielded an 8-bit value that corresponded to the temperature of the sample as read by a thermocouple.

Figure 4 shows the induced temperature change in the Tm^{3+}:ZBLANP sample versus the pump wavelength,

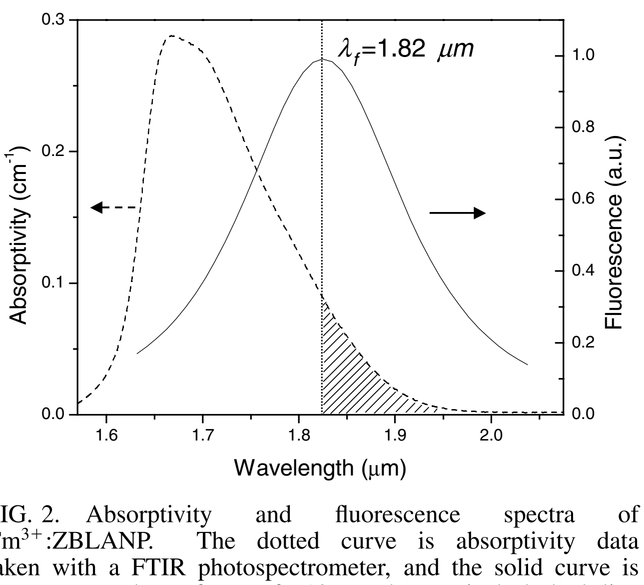

FIG. 2. Absorptivity and fluorescence spectra of Tm^{3+}:ZBLANP. The dotted curve is absorptivity data taken with a FTIR photospectrometer, and the solid curve is fluorescence data after Ref. [10]. The vertical dashed line marks the mean fluorescent wavelength at 1.82 μm, and the shaded area indicates the pump wavelength region where cooling is expected.

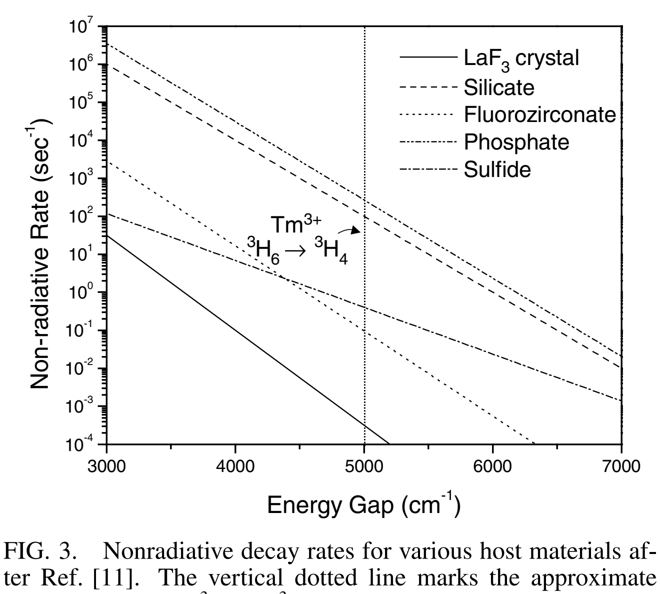

FIG. 3. Nonradiative decay rates for various host materials after Ref. [11]. The vertical dotted line marks the approximate energy gap for the $^3H_6 \rightarrow {}^3H_4$ transitions most relevant to nonradiative decay considerations for Tm^{3+} ions in these hosts.

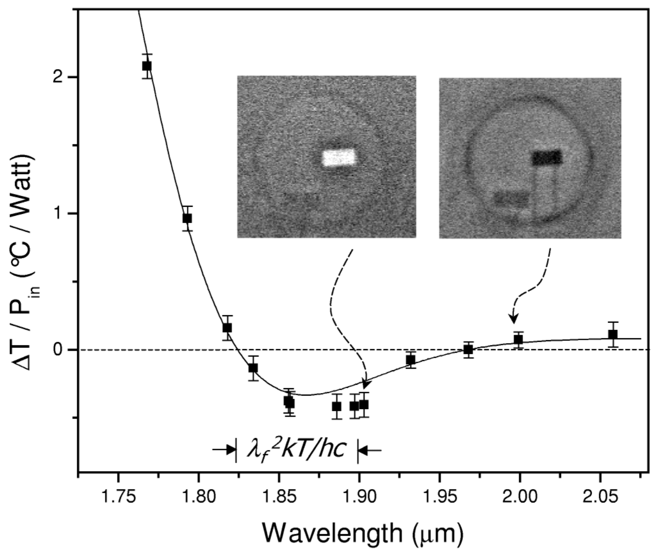

FIG. 4. Temperature change, normalized to incident power, versus pump wavelength for a Tm^{3+}:ZBLANP sample. The insets are two thermal images corresponding to 1.9 μm (cooling) and 2.0 μm (heating). Bright areas indicate cooling and dark areas indicate heating. Note the residual heating of the chamber walls, reference sample at lower left, and the glass support slides. The solid line is a theoretical fit using Eq. (2), and the marked $\Delta\lambda$ corresponds to $h\nu_f - h\nu = kT$ at room temperature.

where temperature change is normalized to incident pump power. At a pump wavelength of 1.9 μm and incident average power of $\sim$3 W, the sample cooled to -1.2 °C below room temperature for a single pass of the pump beam through the sample. This corresponds to an absorbed power of $\sim$40 mW and therefore a peak cooling per absorbed power of ~ -30 °C/W. The heating at wavelengths longer than $\sim$2 μm can be attributed to parasitic background absorption from unwanted impurities in the glass such as transition metals. Modeling this absorption by a wavelength independent coefficient α_b, the normalized temperature change of the sample can be expressed as

$$\frac{\Delta T}{P_{\text{in}}} = \kappa\left[\alpha_b - \alpha_r(\lambda)\,\frac{\lambda - \lambda_f}{\lambda_f}\right], \tag{2}$$

where $\alpha_r(\lambda)$ is the resonant absorption coefficient as depicted in Fig. 2, P_{in} is the incident pump power, and κ is a constant that includes sample length and depends on thermodynamic factors such as radiative load from the chamber walls and conduction through the glass support slides and remaining gas in the chamber. Equation (2) is valid in the limit of low absorption (see Fig. 2). The solid curve in Fig. 4 is a theoretical fit based on Eq. (2) with $\lambda_f = 1.82$ μm, $\kappa \simeq 406$ °C cm/W, and $\alpha_b = 0.0002$ cm^{-1}. The resonant absorption coefficient, $\alpha_r(\lambda)$, is a functional fit to the experimental absorption data that is made to approach zero at long wavelengths. Despite the amount of implicit background absorption found from the fit, the anti-Stokes cooling dominates between $\sim$1.82 and 1.97 μm.

To investigate the effect of nonradiative decay we generalize Eq. (2) to include fluorescence quenching. This effect is manifested as nonunity quantum efficiency and results in additional heating that follows resonant absorption. Including this, we can express to first order the normalized change in temperature of the sample as

$$\frac{\Delta T}{P_{\text{in}}} = \kappa\left[\alpha_b + \alpha_r(\lambda)(1 - \eta_q) - \alpha_r(\lambda)\eta_q\,\frac{\lambda - \lambda_f}{\lambda_f}\right], \tag{3}$$

where η_q is the quantum efficiency for the Tm^{3+} ions in the host material. Using Eq. (3) to fit our data we find that the sample has a quantum efficiency of greater than 99%.

Since quantum efficiency is related to atomic lifetimes, Eq. (3) gives an upper limit on the nonradiative decay rate (R_{nr}) allowed in the cooling process for a given pump wavelength. Quantum efficiency is defined as $(1 + R_{\text{nr}}\tau_{\text{rad}})^{-1}$, where τ_{rad} is the radiative lifetime. Assuming no background absorption, by Eq. (3) we see that to observe cooling the material must meet the condition

$$R_{\text{nr}}\tau_{\text{rad}} < \frac{\lambda - \lambda_f}{\lambda_f}. \tag{4}$$

With the measured value of $\tau_{\text{rad}} = 6.2$ ms [11], we find $R_{\text{nr}} \lesssim 3$ s^{-1} for $\lambda_f = 1.82$ μm and $\lambda = 1.86$ μm. According to Fig. 3, the fluorozirconate host safely meets this criterion while silicate and phosphate do not.

The sensitivity of the expected cooling to wavelength-independent background absorption is shown in Fig. 5, where Eq. (2) is plotted again with four different values of α_b. Background absorption corresponding to $\alpha_b > 0.001$ cm^{-1} eliminates net cooling for our sample.

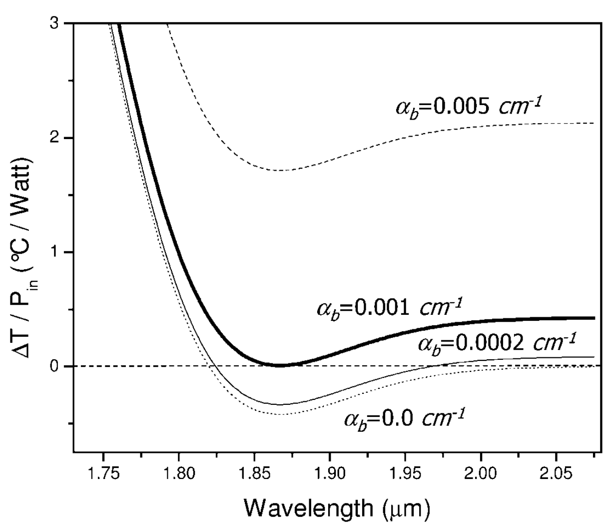

FIG. 5. Plots of Eq. (2) with the same parameters as in the fit of Fig. 4 for different values of background absorption coefficient (α_b). The dotted curve at bottom corresponds to $\alpha_b = 0.0$ cm^{-1}, the solid curve to $\alpha_b = 0.0002$ cm^{-1} (used to fit our data), the thick solid curve to $\alpha_b = 0.001$ cm^{-1}, and the dashed curve at top to $\alpha_b = 0.005$ cm^{-1}.

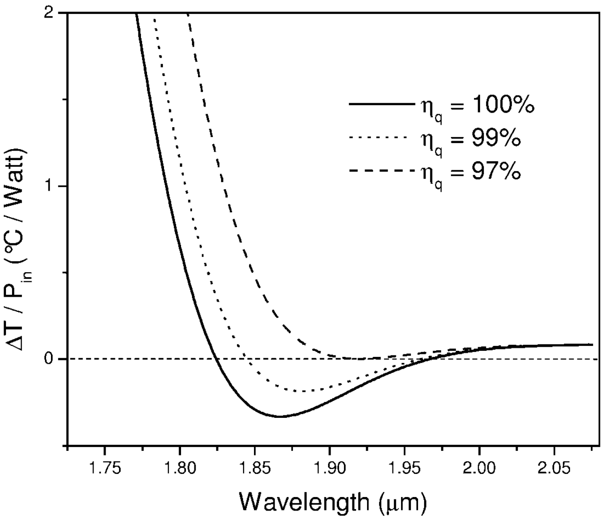

FIG. 6. Plots of Eq. (3) with the same parameters as in the fit of Fig. 4 for different values of quantum efficiency (η_q). The solid curve at bottom corresponds to $\eta_q = 100\%$ [Eq. (2)], the dotted curve to $\eta_q = 99\%$, and the dashed curve at top to $\eta_q = 97\%$.

Similarly, the sensitivity of the cooling process to quantum efficiency (η_q) is shown in Fig. 6, where Eq. (3) is plotted with three different values of η_q for $\alpha_b = 0.0002$ cm^{-1}. Quantum efficiencies less than ~97% eliminate cooling for our sample. In other experiments we examined different thulium-doped solids and found no cooling. These solids included Tm^{3+}:CaF_2, Tm^{3+}:BaF_2, and another sample of Tm^{3+}:ZBLANP. These negative results can be attributed to background absorption or fluorescence quenching by impurities or defects as discussed above.

Similar to the cooling transitions discussed above, excitations to the $^3F_4$ manifold in the Tm^{3+}:ZBLANP sample have the potential to produce fluorescence cooling. Along the possible decay paths from this manifold, the $^3F_4 \rightarrow {}^3H_5$ and the decays are largely radiative (see Fig. 3). However, the $^3H_5 \rightarrow {}^3H_4$ transition is strongly nonradiative. Nevertheless, the branching ratio for the $^3F_4 \rightarrow {}^3H_5$ transition of 0.03 [11] indicates that the heat from this nonradiative branch should be small compared to the cooling processes. Since the $^3F_4$ manifold lies 6900 cm^{-1} above the $^3H_4$ level, it can be populated via excited-state absorption (ESA) during illumination by the OPO at $1.82 < \lambda < 1.97$ μm. This was verified by observing fluorescence at ~1 μm using a simple silicon-based video camera during our experiments. At the above excitation wavelengths, this ESA process is endothermic and should contribute extra cooling if fluorescence efficiency and background absorption are in the acceptable range. Since our average intensity is far below the saturation intensity of the $^3H_4 \rightarrow {}^3F_4$ transition, we expect the population of the $^3H_4$ manifold to be much larger than that of the $^3F_4$ manifold. Therefore any heating or cooling effects from the ESA process should be negligible. We examined the $^3F_4$ manifold further by directly pumping the $^3H_6 \rightarrow {}^3F_4$ transition using a Ti:sapphire laser at 790–900 nm. We did not, however, observe any cooling. This may indicate the presence of strong fluorescence quenching at this transition in addition to the background absorption.

In conclusion, we have presented the first observation of optical cooling in a Tm^{3+}-doped solid. We used tunable near-infrared light from an OPO to cool a sample by −1.2 °C from room temperature for a single pass of the pump beam. We deduce a peak cooling per absorbed power of ~ − 30 °C/W, which depends on the thermal load to the sample—this value can be drastically improved by reducing the surface area of the sample and covering the vacuum chamber walls with low thermal emissivity materials [3]. By increasing the absorbed power via pump recycling (as in mirrored samples [3]) and using higher doping concentrations we should be able to approach cryogenic temperatures in this material with our available laser power.

The authors gratefully acknowledge the financial support of a NUCOR grant awarded by the University of California. We also thank Majid Ebrahimzadeh (University of St. Andrews) and Nathan Brilliant (University of New Mexico) for their assistance in the design of the OPO, and the University of New Mexico NASA/PURSUE program for supporting an undergraduate student (Ameer Bauer) to assist in this project.

*Electronic address: hoycha@unm.edu

[1] R. I. Epstein, M. I. Buchwald, B. C. Edwards, T. R. Gosnell, and C. E. Mungan, Nature (London) **377**, 500 (1995).

[2] J. L. Clark and G. Rumbles, Phys. Rev. Lett. **76**, 2037 (1996).

[3] B. C. Edwards, J. E. Anderson, R. I. Epstein, G. L. Mills, and A. J. Mord, J. Appl. Phys. **86**, 6489 (1999).

[4] B. C. Edwards, M. I. Buchwald, and R. I. Epstein, Rev. Sci. Instrum. **69**, 2050 (1998).

[5] T. R. Gosnell, Opt. Lett. **24**, 1041 (1999).

[6] C. E. Mungan, M. I. Buchwald, B. C. Edwards, R. I. Epstein, and T. R. Gosnell, Appl. Phys. Lett. **71**, 1458 (1997).

[7] H. Gauck, T. H. Gfroerer, M. J. Renn, E. A. Cornell, and K. A. Bertness, Appl. Phys. A **64**, 143 (1997).

[8] E. Finkeissen, M. Potemski, P. Wyder, L. Vina, and G. Weimann, Appl. Phys. Lett. **75**, 1258 (1999).

[9] J. Y. Allain, M. Monerie, and H. Poignant, Electron. Lett. **25**, 1660 (1989).

[10] J. N. Carter, R. G. Smart, D. C. Hanna, and A. C. Tropper, Electron. Lett. **26**, 599 (1990).

[11] W. J. Miniscalco, in *Rare Earth Doped Fiber Lasers and Amplifiers,* edited by M. J. F. Digonnet (Marcel Dekker, New York, 1993), p. xv.

[12] C. W. Hoyt, A. Bauer, and M. Sheik-Bahae, in *Opto-Southwest, Proceedings of the SPIE Regional Meeting, Albuquerque, NM, 2000* (International Society for Optical Engineering, Bellingham, WA, 2000).